Received: 7 May 2020 | Revised: 28 June 2020 | Accepted: 1 July 2020

DOI: 10.1111/mmi.14571

RESEARCH ARTICLE

WILEY

Depletion of the DarG antitoxin in *Mycobacterium tuberculosis* triggers the DNA-damage response and leads to cell death

Anisha Zaveri[1] | Ruojun Wang[1] | Laure Botella[1] | Ritu Sharma[1] | Linnan Zhu[1] | Joshua B. Wallach[1] | Naomi Song[1] | Robert S. Jansen[2] | Kyu Y. Rhee[2] | Sabine Ehrt[1] | Dirk Schnappinger[1]

[1]Department of Microbiology and Immunology, Weill Cornell Medicine, New York, NY, USA

[2]Department of Medicine, Weill Cornell Medicine, New York, NY, USA

Correspondence
Dirk Schnappinger, Department of Microbiology and Immunology, Weill Cornell Medicine, New York, NY, USA.
Email: dis2003@med.cornell.edu

Present address
Laure Botella, Host-Pathogen Interactions in Tuberculosis Laboratory, The Francis Crick Institute, London, UK
Ritu Sharma, AveXis Inc., 2275 Half Day Road, Suite 200, Bannockburn, IL, USA
Linnan Zhu, BGI-Shenzhen, Shenzhen, China
Naomi Song, School of Nursing, University of Pennsylvania, Philadelphia, PA, USA
Robert S. Jansen, Department of Microbiology, Radboud University, Nijmegen, Netherlands

Funding information
This work was supported by the Tri-Institutional TB Research Unit (NIH grant U19 AI111143) and NIH grant U19 A107774.

Abstract

Of the ~80 putative toxin-antitoxin (TA) modules encoded by the bacterial pathogen *Mycobacterium tuberculosis* (*Mtb*), three contain antitoxins essential for bacterial viability. One of these, Rv0060 (DNA ADP-ribosyl glycohydrolase, $DarG_{Mtb}$), functions along with its cognate toxin Rv0059 (DNA ADP-ribosyl transferase, $DarT_{Mtb}$), to mediate reversible DNA ADP-ribosylation (Jankevicius *et al*., 2016). We demonstrate that $DarT_{Mtb}$-$DarG_{Mtb}$ form a functional TA pair and essentiality of $darG_{Mtb}$ is dependent on the presence of $darT_{Mtb}$, but simultaneous deletion of both $darT_{Mtb}$-$darG_{Mtb}$ does not alter viability of *Mtb* in vitro or in mice. The antitoxin, $DarG_{Mtb}$, forms a cytosolic complex with DNA-repair proteins that assembles independently of either $DarT_{Mtb}$ or interaction with DNA. Depletion of $DarG_{Mtb}$ alone is bactericidal, a phenotype that is rescued by expression of an orthologous antitoxin, $DarG_{Taq}$, from *Thermus aquaticus*. Partial depletion of $DarG_{Mtb}$ triggers a DNA-damage response and sensitizes *Mtb* to drugs targeting DNA metabolism and respiration. Induction of the DNA-damage response is essential for *Mtb* to survive partial $DarG_{Mtb}$-depletion and leads to a hypermutable phenotype.

KEYWORDS

DNA damage, *Mycobacterium tuberculosis*, toxin-antitoxin systems

1 | INTRODUCTION

Toxin-antitoxin (TA) systems are ubiquitously present in prokaryotic genomes and consist of a toxic protein that inhibits an essential cellular process and a counteracting antitoxin that binds to and neutralizes the toxin (Yamaguchi *et al*., 2011). TA systems were originally discovered due to their ability to prevent plasmid loss by post-segregational killing (Ogura and Hiraga, 1983; Gerdes *et al*., 1986). They have subsequently been implicated in various cellular pathways including phage defense, genome stabilization, and bacterial persistence (Szekeres *et al*., 2007; Gerdes and Maisonneuve, 2012; Harms *et al*., 2018).

The phyletic distribution of TA modules indicates that *Mycobacterium tuberculosis* (*Mtb*), the causative agent of tuberculosis, harbors an expanded repertoire of 79 putative TA loci (Pandey and Gerdes, 2005; Sala *et al*., 2014; Slayden *et al*., 2018). Individual deletions of many of these TA loci exhibit few, if any phenotypic defects, likely due to functional redundancy (Singh *et al*., 2010; Tiwari

et al., 2015). However, 3 of the 79 TA modules in *Mtb* harbor antitoxins that are essential for viability of the organism, namely Rv0060, Rv1044, and Rv1990c (DeJesus *et al*., 2017). Rv1044 is uncharacterized, and Rv1990c was recently identified as MbcA, an antitoxin that neutralizes a NAD^+ phosphorylase toxin, MbcT (Freire *et al*., 2019). Rv0060 ($DarG_{Mtb}$), and its cognate toxin, Rv0059 ($DarT_{Mtb}$), are the focus of this study.

Within mycobacteria, the *darT-darG* locus is found only in species belonging to the *Mtb* complex (Kanehisa and Goto, 2000). However, orthologous genes have been identified in the extremophile *Thermus aquaticus* (*Taq*) and in enteropathogenic *E. coli* (EPEC) (Jankevicius *et al*., 2016; Lawaree *et al*., 2020). In vitro experiments established that $DarT_{Taq}$, $DarT_{Ec}$, and $DarT_{Mtb}$ can ADP-ribosylate single stranded DNA at thymidine residues (Jankevicius *et al*., 2016; Lawaree *et al*., 2020). In both *E. coli* and *T. aquaticus*, the antitoxin, DarG, physically interacts with DarT, leading to toxin neutralization. In addition, $DarG_{Taq}$, $DarG_{Ec}$, and $DarG_{Mtb}$ can enzymatically reverse the action of their cognate toxins by removal of the ADP-ribose moiety (Jankevicius *et al*., 2016; Lawaree *et al*., 2020). Taken together, biochemical characterization demonstrates that $DarT_{Mtb}$-$DarG_{Mtb}$ mediate reversible ADP-ribosylation of DNA (Jankevicius *et al*., 2016).

While the biological roles of $DarT_{Mtb}$-$DarG_{Mtb}$ remain unknown, in vivo studies performed on the orthologous *E. coli* DarTG system find that ADP-ribosylation by $DarT_{Ec}$ halts DNA replication. The resulting DNA lesions are repaired by two DNA-repair pathways: RecF-mediated homologous recombination and nucleotide excision repair (Lawaree *et al*., 2020). In this study, we characterize the *Mtb* orthologs of the DarTG system by delineating the cellular processes affected by genetic perturbation of the $darT_{Mtb}$-$darG_{Mtb}$ locus.

2 | RESULTS

2.1 | $DarT_{Mtb}$ and $DarG_{Mtb}$ form a toxin-antitoxin pair that is dispensable for growth in vitro, growth in mice, persistence in mice, and resistance to various stresses

Tn-seq studies predicted that $darG_{Mtb}$ is essential for growth in *Mtb* (DeJesus *et al*., 2017). We asked if the essentiality of $darG_{Mtb}$ was dependent on the presence of $darT_{Mtb}$. We attempted to generate a deletion strain of both *darT* and *darG* in *Mtb* by replacement of the native locus with a hygromycin resistance cassette. We failed to obtain mutant colonies, suggesting that $darG_{Mtb}$ could be essential even when $darT_{Mtb}$ was absent (Figure 1a, top row). To test this, we used an alternate strategy to obtain $\Delta darT_{Mtb}$-$darG_{Mtb}$. First, we generated a strain that contained a second copy of $darG_{Mtb}$ on an *attL5*-integrating plasmid with a streptomycin resistance cassette (Figure 1a, middle row). In this merodiploid we then successfully replaced the native $darT_{Mtb}$-$darG_{Mtb}$ locus with a hygromycin resistance cassette (Figure 1a, bottom row). Resident plasmids at the *attL5* site can be efficiently switched with another *attL5*-integrating plasmid containing a different

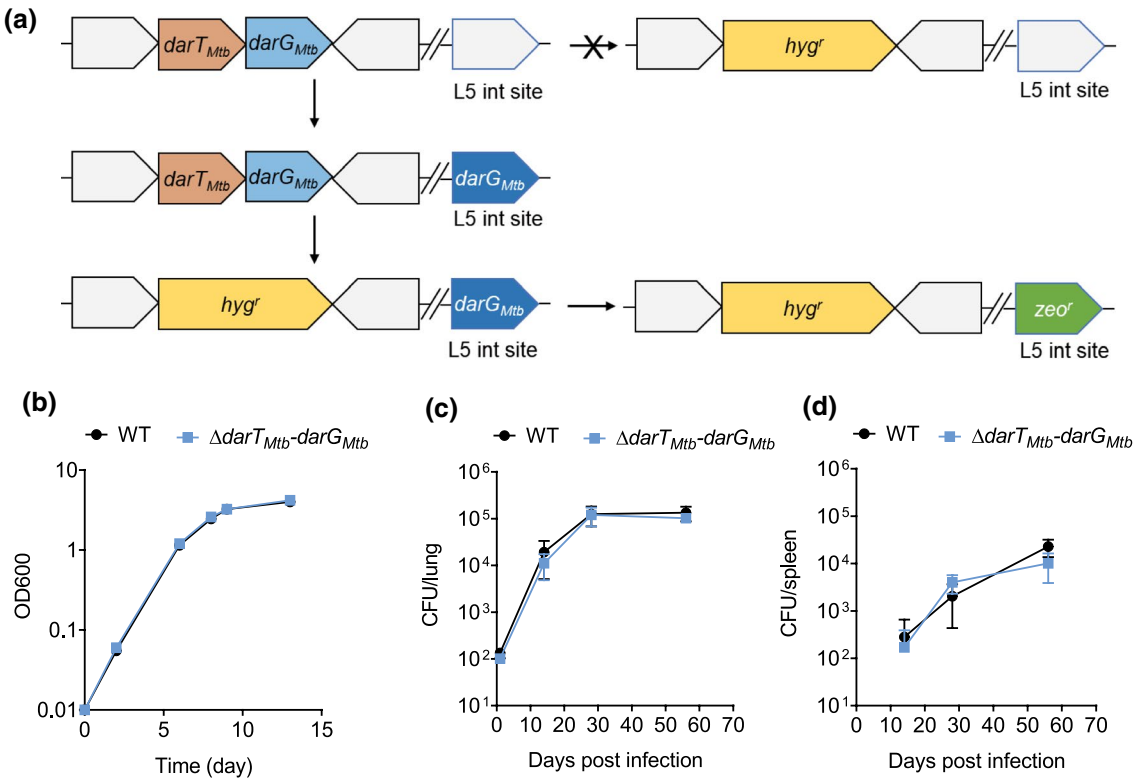

FIGURE 1 Generation and growth of $\Delta darT_{Mtb}$-$darG_{Mtb}$ in vitro and in vivo. (a) Schematic depicting generation of $\Delta darT_{Mtb}$-$darG_{Mtb}$. (b) Growth of WT and $\Delta darT_{Mtb}$-$darG_{Mtb}$ in 7H9 media as measured by optical density. (c and d) Quantification of bacterial loads in (c) lungs and (d) spleens of C56BL/6 mice infected with WT or $\Delta darT_{Mtb}$-$darG_{Mtb}$ *Mtb*. Data are mean ± *SD* of four mice per group

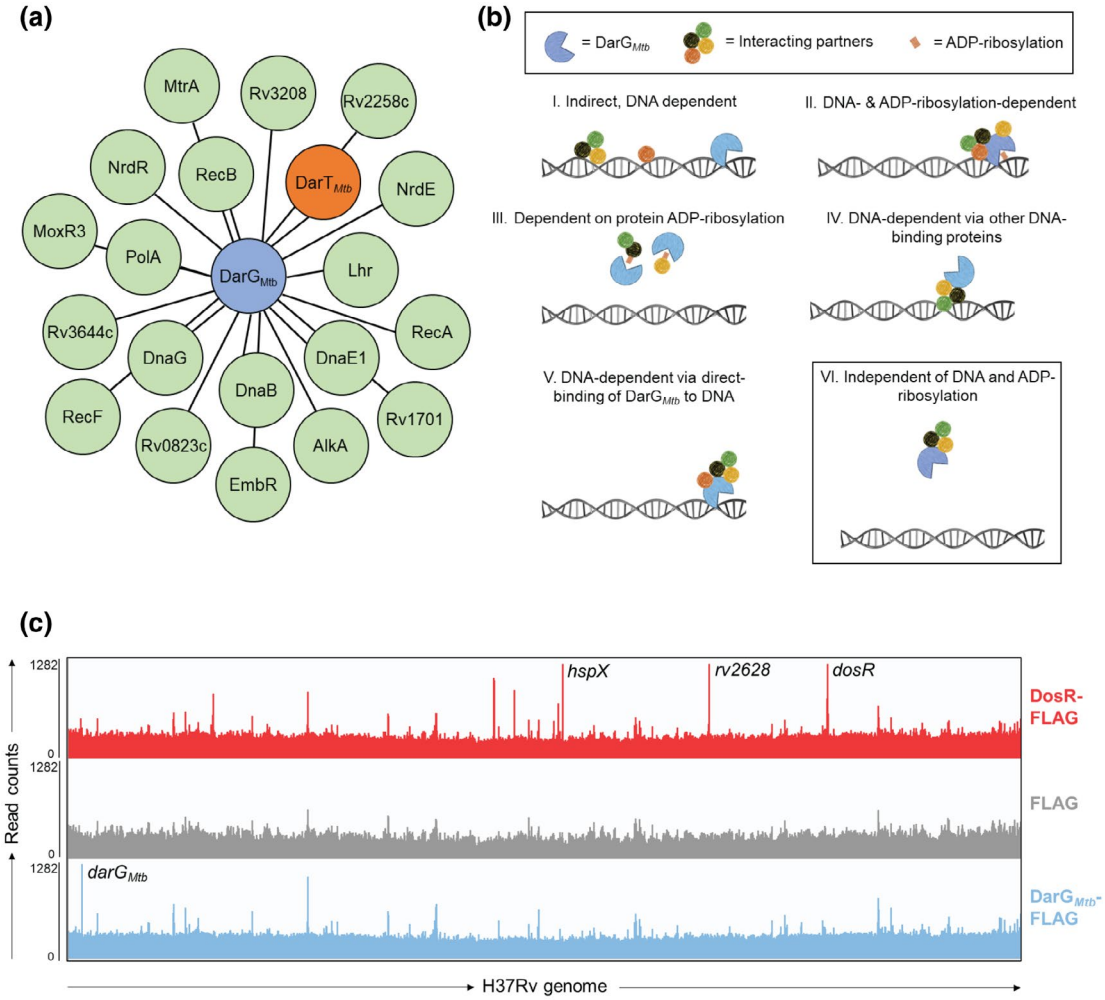

FIGURE 2 DarG$_{Mtb}$ interacts with DarT$_{Mtb}$ and with proteins involved in DNA replication and repair. (a) Network map of selected interacting partners of DarG$_{Mtb}$. DarT$_{Mtb}$ is marked in orange. (b) Schematics displaying possible modes of interaction between DarG$_{Mtb}$ (blue), DNA-binding proteins (colored circles), and DNA. ADP-ribosylation is represented by a brown line. The most plausible model is boxed. (c) Raw read counts from chromatin immunoprecipitation experiments for DosR-FLAG, FLAG-control, and DarG$_{Mtb}$-FLAG plotted against the *Mtb* H37Rv genome coordinate. Peaks within selected genes are annotated. Data are representative of three independent replicates

antibiotic-resistance cassette (Pashley and Parish, 2003). Hence, we transformed the Δ*darT*$_{Mtb}$-*darG*$_{Mtb}$::*darG*$_{Mtb}$ strain with an *attL5*-integrating plasmid conferring zeocin-resistance but not expressing any *Mtb* gene. We successfully obtained zeocin-resistant colonies (Figure 1a, bottom row). We confirmed the resulting Δ*darT*$_{Mtb}$-*darG*$_{Mtb}$ mutant by Southern blotting (Figure S1). Δ*darT*$_{Mtb}$-*darG*$_{Mtb}$ exhibited no growth defect in standard 7H9 media (Figure 1b) and showed growth and survival comparable to WT following infection of C57B/6 mice (Figure 1c–1d). The mutant also failed to show a phenotype when subjected to various stressors including the antibiotics isoniazid, rifampicin, ciprofloxacin, levofloxacin, the anticancer drug mitomycin C (used as a DNA damaging agent; Iyer and Szybalski, 1963), starvation, nitric oxide, and H_2O_2 (Figure S2).

These findings establish that the essentiality of *darG*$_{Mtb}$ is dependent on the presence of *darT*$_{Mtb}$ and confirm that the two form a toxin-antitoxin pair. Toxicity from residual DarT$_{Mtb}$ protein in the cytoplasm likely explains our failure to obtain the Δ*darT*$_{Mtb}$-*darG*$_{Mtb}$ mutant by direct replacement in the WT strain.

2.2 | DarG$_{Mtb}$ interacts with DarT$_{Mtb}$ and with proteins involved in DNA replication and repair

It is common for antitoxin proteins to inhibit their cognate toxins by direct protein–protein interactions (Yamaguchi *et al*., 2011). Hence, we expressed and immunoprecipitated a FLAG-tagged version of DarG$_{Mtb}$ in WT *Mtb* and identified interacting proteins by mass spectrometry. Indeed, we found that DarG$_{Mtb}$ bound to DarT$_{Mtb}$ (Figure 2a, Table 1). In addition, 9 of the top 20 hits were proteins related to DNA metabolism. Specifically, we identified interactions between DarG$_{Mtb}$ and members of the mycobacterial replisome including the replicative polymerases (DnaE1, PolA), helicase (DnaB), and primase (DnaG). DNA-repair-associated proteins such as RecA, RecB, RecF, Lhr, and AlkA were also part of the DarG$_{Mtb}$ interactome (Figure 2a, Table 1, and S1). We then tested if the association of DarG$_{Mtb}$ was dependent on an interaction with DNA or the ribosylation of DNA or proteins (Figure 2b). For example, co-precipitation of DarG$_{Mtb}$ with any DNA-binding protein could

TABLE 1 $DarG_{Mtb}$ interacts with proteins involved in DNA replication and repair

Rank	Rv	Gene	Description	iP: $DarG_{Mtb}$ in WT	iP: $DarG_{Mtb}$ in WT + DNaseI	iP: $DarG_{Mtb}$ in DKO
1	Rv3296	*lhr*	Probable ATP-dependent helicase Lhr	22.75	18.5	18
2	Rv1547	*dnaE1*	Probable DNA polymerase III DnaE1	18.75	15	23
3	Rv0058	*dnaB*	Probable replicative DNA helicase DnaB	15.5	7.5	6
4	Rv2343c	*dnaG*	Probable DNA primase DnaG	20.25	15.5	9.5
7	Rv0059	*darT*	DNA ADP-ribosyl transferase DarT	24	31	0.9
10	Rv1629	*polA*	Probable DNA polymerase I PolA	12	14	9.5
12	Rv0630c	*recB*	Probable exonuclease V (beta chain) RecB	11.25	5	5
16	Rv3051c	*nrdE*	Ribonucleoside-diphosphate reductase NrdE	14.5	18.5	30
18	Rv2737c	*recA*	RecA protein (recombinase A)	33.5	27.5	33.5
22	Rv3208	*rv3208*	Probable transcriptional regulatory protein (probably TetR-family)	8.5	11	9
30	Rv1701	*rv1701*	Probable integrase/ recombinase	16.25	9	6.5
34	Rv1317c	*alkA*	Probable bifunctional regulatory protein and DNA-repair enzyme AlkA	7.25	5.5	4.5
47	Rv1267c	*embR*	Probable transcriptional regulatory protein EmbR	15.25	17.5	12.5
57	Rv0823c	*rv0823c*	Possible transcriptional regulatory protein	7.75	8	5
61	Rv0003	*recF*	DNA replication and repair protein RecF	9.25	8	5.5
62	Rv2258c	*rv2258c*	Possible transcriptional regulatory protein	8.75	10.5	10.5
65	Rv3644c	*rv3644c*	Possible DNA polymerase	10.25	9	5.5
66	Rv1446c	*opcA*	Putative OXPP cycle protein OpcA	12	7	7
67	Rv3164c	*moxR3*	Probable methanol dehydrogenase transcriptional regulatory protein MoxR3	8	5.5	4
90	Rv2718c	*nrdR*	Probable transcriptional regulatory protein NrdR	8.25	8.5	9
91	Rv3246c	*mtrA*	Two component sensory transduction transcriptional regulatory protein MtrA	9	9	13

Note.: Rank, names, and average total spectrum counts of DNA metabolism-related proteins identified to interact with $DarG_{Mtb}$ are displayed. $DarG_{Mtb}$-FLAG was immunoprecipitated (iP) from whole-cell lysates of WT or $\Delta darT_{Mtb}$-$darG_{Mtb}$ (DKO) *Mtb* strains transformed with plasmids encoding $DarG_{Mtb}$-FLAG under a constitutive promoter. "$DarG_{Mtb}$ in WT + DNaseI" represents data from WT lysates treated with DNaseI post iP. Interacting proteins were identified by mass spectrometry. Data were calculated from four biological replicates (iP: $DarG_{Mtb}$ in WT) or biological duplicates (iP: $DarG_{Mtb}$ in WT + DNaseI, iP: $DarG_{Mtb}$ in DKO). Biological duplicates of WT *Mtb* and an experiment with WT *Mtb* overexpressing a FLAG tag were used as controls. Nonspecific binding peptides were removed from the results by setting the filter of "Total Spectrum Count" of each replicate to "≤4" in the control samples and "≥5" in "$DarG_{Mtb}$ in WT" samples. Hits were ranked in descending order based on the ratio of average total spectrum count of "$DarG_{Mtb}$ in WT" versus controls, with the corresponding rank indicated in the "Rank" column. Unfiltered raw counts are available in the Supporting Information (Table S1).

potentially be explained by the presence of complexes containing DNA bound independently to $DarG_{Mtb}$ and to resident DNA-binding proteins (Figure 2b, Model I). To test this, we repeated the pull-down on DNase-treated lysates. We did not find a substantial difference in the protein-binding profile of $DarG_{Mtb}$ with or without DNase treatment (Table 1), thus, ruling out Model I. Next, we conjectured that $DarG_{Mtb}$ might recruit DNA-repair proteins on recognition and binding to an ADP-ribosylated base (Figure 2b, Model II). Our results could also be explained by ADP-ribosylation of the interacting proteins themselves (Figure 2b, Model III). We tested these possibilities by repeating the pull-down in a strain lacking $DarT_{Mtb}$, and therefore, presumably lacking ADP-ribosylation. Interactions between $DarG_{Mtb}$ and DNA metabolism proteins persisted even in the absence of $DarT_{Mtb}$. In short, $DarG_{Mtb}$ bound to DNA metabolism-related proteins in a $DarT_{Mtb}$-independent manner.

Finally, we examined if $DarG_{Mtb}$ either co-localized with (Figure 2b, Model IV) or directly bound to DNA (Figure 2b, Model V). We performed microscopy using $DarG_{Mtb}$-mCherry and SYTO13-labeled DNA (Figure S3). We observed variable localization of $DarG_{Mtb}$-mCherry. Specifically, 44% of bacteria contained $DarG_{Mtb}$-mCherry foci which did not overlap with SYTO13-labeled DNA. The remaining bacteria contained diffuse mCherry signals (Figure S3). Since these results were inconclusive, we performed chromatin immunoprecipitation (ChIP-seq) using an anti-FLAG antibody on lysates of WT *Mtb* expressing $DarG_{Mtb}$-FLAG, DosR-FLAG (positive control), or the FLAG tag alone (negative control). Compared to the FLAG tag control, there was little or no enrichment of read counts in the $DarG_{Mtb}$-FLAG ChIP (Figure 2c; no significant differentially bound sites detected using DiffBind (Stark and Brown, 2011)), with the exception of a peak mapping to $darG_{Mtb}$. Since these read counts are not normalized to the ChIP input, this peak is likely an artifact originating from the multicopy episomal plasmid encoding $DarG_{Mtb}$-FLAG. In contrast, enriched peaks of known DosR targets, *hspX* and *rv2628*, were detected in the DosR ChIP (Figure 2c). While we cannot rule out short-lived and/or nonsequence-specific interactions with DNA that would be undetectable by ChIP-seq, these data demonstrate that $DarG_{Mtb}$ likely forms a cytosolic complex with DNA-repair proteins that assembles independently of an interaction with DNA (Figure 2b, Model VI).

2.3 | $DarG_{Mtb}$-depletion triggers cell death which is prevented by its *T. aquaticus ortholog*

Next, we sought to understand the downstream effects of $DarT_{Mtb}$ expression. We were unable to overexpress $DarT_{Mtb}$ in *Mtb*, since its toxicity in *E. coli* precluded our attempts to clone the gene, similar to previous attempts (Jankevicius *et al*., 2016). Instead, we generated an anhydrotetracycline (ATC)-controlled knockdown strain of $darG_{Mtb}$ with the expectation that $DarG_{Mtb}$-depletion would phenocopy overexpression of $darT_{Mtb}$. Briefly, we achieved proteolytic control of native $DarG_{Mtb}$ by its fusion to a carboxy-terminal DAS-tag. DAS-tagged proteins are targeted to the ClpP protease by adapter protein SspB, which was expressed under the control of the reverse Tet repressor (Kim *et al*., 2011). In the resulting $darG_{Mtb}$-TetON strain, removal of ATC led to a decrease in the expression of $DarG_{Mtb}$ which was accompanied by cell death (Figure 3a-b). The toxicity associated with $DarG_{Mtb}$-depletion was fully rescued by constitutive expression of either $DarG_{Mtb}$, or its ortholog from *T. aquaticus*, $DarG_{Taq}$ (Figure 3c). Mutation of K80 in $DarG_{Taq}$ abrogates the protein's de-ADP-ribosylation activity (Jankevicius *et al*., 2016). In concordance with this, a K80A mutant of $DarG_{Taq}$ failed to rescue ATC-dependent growth of $darG_{Mtb}$-TetON (Figure 3c). Finally, we examined the consequences of overexpressing $DarT_{Taq}$ in *Mtb*. We transformed $\Delta darT_{Mtb}$-$darG_{Mtb}$ with a plasmid encoding $darT_{Taq}$ under an ATC-inducible promoter. The resulting strain was unable to grow when exposed to ATC, a phenotype that was rescued by constitutive expression of $DarG_{Mtb}$ (Figure 3d). Overall, these data establish that the $DarT_{Mtb}$-$DarG_{Mtb}$ toxin-antitoxin system is cross-complemented by $DarT_{Taq}$-$DarG_{Taq}$, thus signifying functional conservation.

Since we were unable to detect binding of $DarG_{Mtb}$ to DNA under baseline conditions (Figure 2c), we asked if $DarG_{Mtb}$ bound DNA upon induction of ADP-ribosylation in the cell. We tested this by performing chromatin immunoprecipitation of FLAG-tagged $DarG_{Mtb}$ from cells expressing ATC-inducible $DarT_{Taq}$ (Figure 3d). We found no differences in mapped reads between cells grown with and without ATC (Figure S4; no significant differentially bound sites detected using DiffBind (Stark and Brown, 2011)), indicating that $DarG_{Mtb}$ does not form stable and consistent interactions with DNA even on overexpression of an active DNA ADP-ribosylase.

2.4 | $DarG_{Mtb}$-depletion sensitizes *Mtb* to drugs targeting DNA metabolism and respiration

Next, we tested if targeting $DarG_{Mtb}$ sensitizes *Mtb* to a panel of antibacterial compounds. We measured the MIC of each drug to $darG_{Mtb}$-TetON while simultaneously varying the extent of $DarG_{Mtb}$ knockdown. $DarG_{Mtb}$-depleted (ATC-low) *Mtb* were most susceptible to drugs targeting respiration (bedaquiline), gyrase (ciprofloxacin, levofloxacin), transcription (rifampicin, rifabutin), and causing DNA damage (mitomycin C, netropsin) (Figure 4b,c). In contrast, MICs of drugs inhibiting translation, and cell wall synthesis were largely unaffected by knockdown of $DarG_{Mtb}$ (Figure 4a,c). These data suggest that depletion of $DarG_{Mtb}$ pre-sensitizes the cells to DNA-damage inducing drugs. Thus, inhibition of $DarG_{Mtb}$ likely perturbs cellular pathways involved in respiration and DNA metabolism.

2.5 | $DarG_{Mtb}$-depletion induces the DNA-damage response resulting in increased mutability

To further explore the consequences of $DarG_{Mtb}$-depletion, we used transposon mutagenesis followed by high-throughput sequencing (Tn-seq) in the $darG_{Mtb}$-TetON strain. We generated transposon mutant libraries in *Mtb* in $DarG_{Mtb}$-depleted (ATC-low)

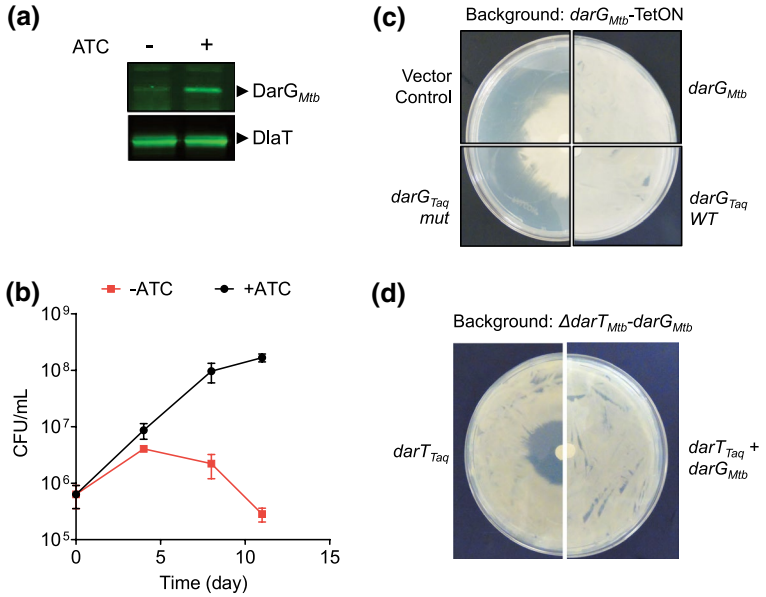

FIGURE 3 DarG$_{Mtb}$-depletion triggers cell death which is prevented by its *T. aquaticus* ortholog. (a) Immunoblot of protein extracts from *darG*$_{Mtb}$-TetON grown with and without ATC. Blot was probed with DarG$_{Mtb}$-specific and DlaT-specific (loading control) antisera (b) Growth of *darG*$_{Mtb}$-TetON quantified by CFU in 7H9 medium with or without ATC. (c) 7H10 agar plates cultured with *darG*$_{Mtb}$-TetON transformed with empty plasmid or plasmids encoding *darG*$_{Mtb}$ WT, *darG*$_{Taq}$ WT, or *darG*$_{Taq}$ mutant expressed from constitutive promoters. The disk in the center of the plate contains 100 ng of ATC; the concentration of ATC decreases from the center to the periphery of the plate. (d) 7H10 agar plates cultured with *ΔdarT*$_{Mtb}$-*darG*$_{Mtb}$ containing a plasmid encoding *darT*$_{Taq}$ from an ATC-inducible promoter transformed with or without a plasmid encoding *darG*$_{Mtb}$ from a constitutive promoter. The disk in the center of the plate contains 800 ng of ATC; the concentration of ATC decreases from the center to the periphery of the plate. Data in (b) are means ± *SD* from three independent experiments. Data in (c-d) are representative of at least two independent experiments

and DarG$_{Mtb}$-replete (ATC-high) conditions. We expressed differences as the log2 fold change (log2FC) of the mutant frequency between libraries exposed to ATC-low and ATC-high conditions. Mutants underrepresented in the ATC-low condition show a negative log2FC and correspond to aggravating genetic interactions with *darG*$_{Mtb}$ (Figure 5a, *left*). In contrast, mutants with a positive log2FC are overrepresented in the ATC-low condition and correspond to alleviating genetic interactions with *darG*$_{Mtb}$ (Figure 5a, *right*).

Aggravating genetic interactions were identified between *darG*$_{Mtb}$ and several genes involved in DNA repair including the master DNA-damage responsive transcriptional activators (*pafBC*), members of the SOS DNA-damage response pathway (*recA* and *recO*), and the helicase involved in nucleotide excision repair (*uvrD1*) (Figure 5a, Table S2) (Fudrini Olivencia *et al*., 2017; Singh, 2017; Muller *et al*., 2018). Importantly, disruption of *darT*$_{Mtb}$ resulted in increased survival of the DarG$_{Mtb}$-depleted strain (Figure 5a, Table S2). In addition, *mma4* and *fecB* exhibited alleviating genetic interactions with *darG*$_{Mtb}$ (Figure 5a, Table S2). Mma4, methoxy mycolic acid synthase 4, is a methyl transferase that modifies cell wall mycolic acids (Yuan and Barry, 1996). FecB is annotated as a putative iron dicitrate-binding lipoprotein, and is a determinant of the intrinsic resistance of *Mtb* to antibiotics (Xu *et al*., 2017). We reasoned that these mutants were favored due to their increased cell wall permeability which allowed greater uptake of ATC in the cell, and consequently, higher expression of DarG$_{Mtb}$ (Dubnau *et al*., 2000; Xu *et al*., 2017).

We also sought to elucidate the transcriptomic changes associated with DarG$_{Mtb}$ knockdown. In agreement with the Tn-seq data, we found that targeting DarG$_{Mtb}$ resulted in a strong induction of genes involved in DNA metabolism (Figure 5b, Table S3). Specifically, we observed a 17-fold upregulation of *dnaE2*, a DNA-damage-induced error-prone translesion polymerase (Boshoff *et al*., 2003). Expression of this gene is associated with an increased mutation frequency and consequently, an increased rate of drug resistance (Boshoff *et al*., 2003). Therefore, we evaluated if targeting DarG$_{Mtb}$ altered the mutation frequency of *Mtb*. We cultured *darG*$_{Mtb}$-TetON in 7H9 media either with (DarG$_{Mtb}$-replete) or without (DarG$_{Mtb}$-depleted) ATC before plating on ATC-containing agar plates with rifampicin. We measured the frequency of rifampicin-resistant *Mtb* as a proxy for the mutability of *darG*$_{Mtb}$-TetON. Indeed, we found that knockdown of DarG$_{Mtb}$ favored the emergence of rifampicin-resistant *Mtb* (Figure 5c). Taken together, these results not only demonstrate that depletion of DarG$_{Mtb}$ induces a DNA-damage response that decreases viability, but also increases mutability.

3 | DISCUSSION

DarG$_{Mtb}$ is one of three putative antitoxins encoded in the *Mtb* genome that is essential for viability (DeJesus *et al*., 2017). Here, we demonstrate that DarT$_{Mtb}$-DarG$_{Mtb}$ indeed form a functional toxin-antitoxin system. Removal of DarG$_{Mtb}$ causes cell death, a phenotype

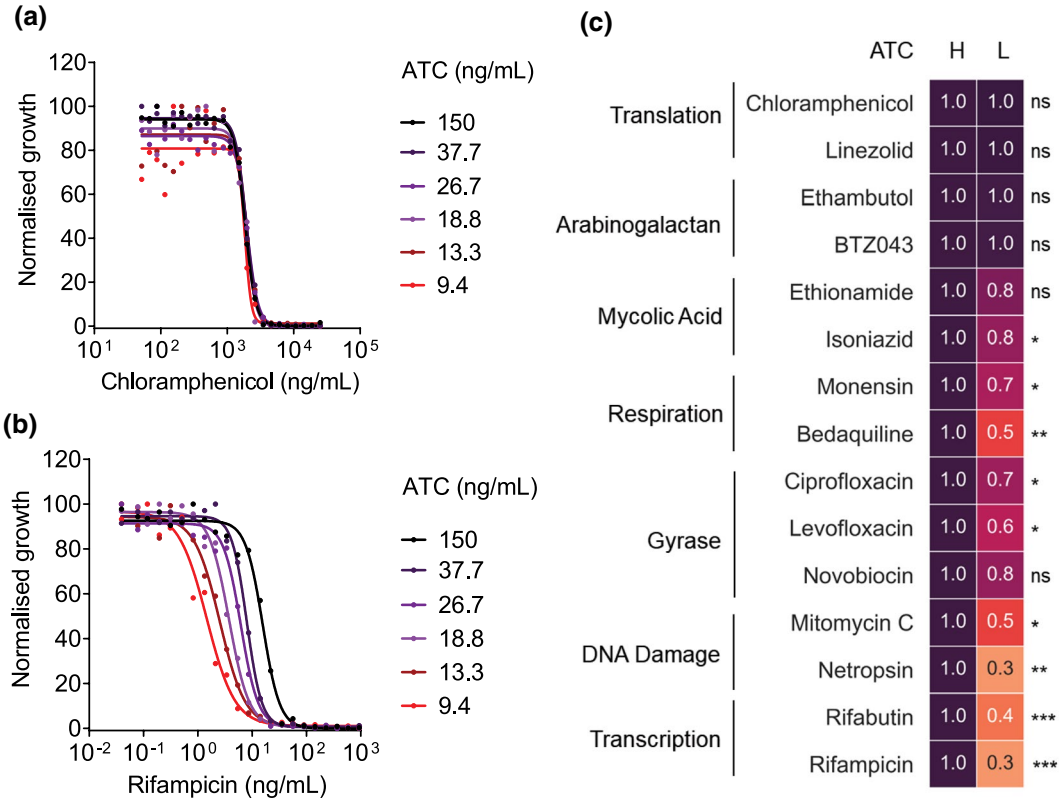

FIGURE 4 DarG$_{Mtb}$-depletion sensitizes *Mtb* to drugs targeting DNA metabolism and respiration. (a and b) Susceptibility of *darG*$_{Mtb}$-TetON to (a) chloramphenicol or (b) rifampicin. *darG*$_{Mtb}$-TetON was cultured in 7H9 medium without ATC for 6 days to decrease DarG$_{Mtb}$ expression before incubating with indicated concentrations of ATC and drug. Growth was measured after 14 days using optical density and normalized to that in the corresponding ATC concentration without drug treatment. (c) Heat-map representation of the MIC$_{50}$ shift of *darG*$_{Mtb}$-TetON to antimicrobial compounds. Experiments were performed as in (a) and (b). Values within each cell are the MIC$_{50}$ for *darG*$_{Mtb}$-TetON grown in high ATC (H; 150 ng/ml) and low ATC (L; concentration of ATC that led to a ~70% growth defect in the absence of drug), normalized to high ATC. Data in (a–b) are representative of three independent experiments. Data in (c) are means calculated from three independent experiments. Symbols on the right indicate results from one-sided *t* test (ns indicates non-significant, * indicates *p* value ≤ 0.05, ** indicates *p* value ≤ 0.01, *** indicates *p* value ≤ .001)

that is rescued by simultaneous deletion of DarT$_{Mtb}$ (Figure 1a, 3b). The mechanism of action of DarT$_{Mtb}$-DarG$_{Mtb}$ is functionally conserved between *Mtb* and *Taq*, as evidenced by cross-complementation experiments (Figure 3c–d). Further, DarT$_{Mtb}$-DarG$_{Mtb}$ physically interact within the cell (Figure 2a, Table 1). However, the role of the DarT$_{Mtb}$-DarG$_{Mtb}$ system in the physiology of *Mtb* remains unknown, as evidenced by the lack of phenotype of the Δ*darT*$_{Mtb}$-*darG*$_{Mtb}$ mutant in a number of physiologically relevant stress conditions (Figure 1b–d, S2). While we cannot discount the possibility of a functionally redundant TA system, the essentiality of DarG$_{Mtb}$ and the uniqueness of DNA ADP-ribosylation argues against this hypothesis. It has been suggested that some TA systems might primarily function to preserve genome integrity (Szekeres *et al*., 2007; Ramage *et al*., 2009), which could be the case for DarT$_{Mtb}$-DarG$_{Mtb}$. Finally, it is possible that the DarT$_{Mtb}$-DarG$_{Mtb}$ TA system plays a role under conditions that are yet untested.

We find that induction of the DNA-damage response is essential for *Mtb* to survive DarG$_{Mtb}$-depletion (Figures 4, 5). Our data are in concordance with observations from EPEC showing that DarT-mediated toxicity is aggravated by disruption of the RecFOR-homologous recombination and nucleotide excision repair pathways (Lawaree *et al*., 2020). Together, these observations support the claim that DarT$_{Mtb}$ primarily exerts its toxicity by ADP-ribosylation of DNA (Jankevicius *et al*., 2016). In addition, DarG$_{Mtb}$ forms cytosolic complexes with several proteins involved in DNA repair, either in a direct or indirect manner (Figure 2a–b, Table 1). This implies that the complex of DarG$_{Mtb}$ with DNA-repair proteins is poised to be recruited to sites of DNA-ADP-ribosylation (Figure 2b, Model VI), where it mediates removal of the ADPr moiety followed by correction of the associated DNA damage. While we failed to detect DarG$_{Mtb}$ bound to DNA, including under conditions that induced ADP-ribosylation (Figures 2c, S4), it is possible that these interactions are too transient or weak to be detected (Nebbioso *et al*., 2017). Alternatively, the binding of DarG$_{Mtb}$ to DNA may lack sequence specificity, which would preclude detection of enriched peaks at a population level.

Importantly, the DNA-damage response triggered by activation of DarT$_{Mtb}$ leads to increased mutability (Figure 5c), possibly due to the induction of DnaE2, a translesion polymerase implicated in the

emergence of drug resistance in vivo (Figure 5b) (Boshoff *et al*., 2003). Transient hypermutability can promote rapid adaptation to novel environments (Taddei *et al*., 1997; Jolivet-Gougeon *et al*., 2011) and promote the evolution of drug resistance (Blazquez, 2003). Thus, induction of hypermutation by dysregulation of the $DarT_{Mtb}$-$DarG_{Mtb}$ complex could be beneficial to a larger population of *Mtb* under unfavorable conditions.

Activation of $DarT_{Mtb}$ has a bactericidal effect (Figure 3b), similar to induction of MbcT, the toxin of the only other characterized TA system in *Mtb* harboring an essential antitoxin (Freire *et al*., 2019).

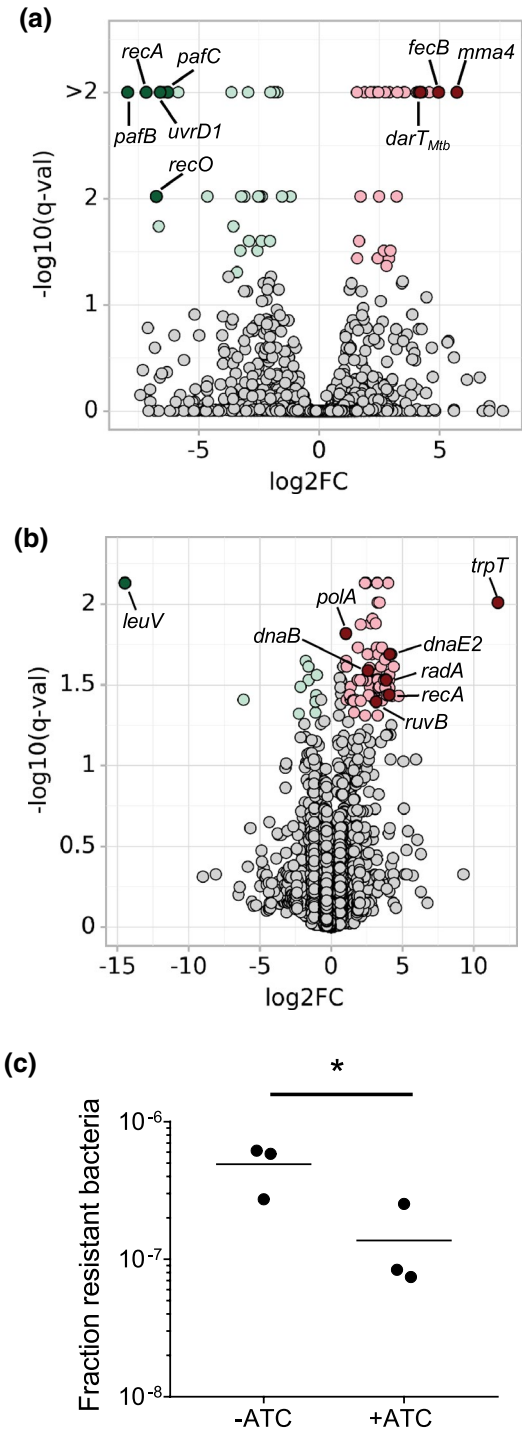

FIGURE 5 $DarG_{Mtb}$-depletion induces the DNA-damage response resulting in increased mutability. (a) Volcano plot representing Tn-seq data from $darG_{Mtb}$-TetON grown on 7H10 agar with low or high ATC. Tn-seq log2FC (low ATC/high ATC) and false discovery rate-adjusted *p* values (*q*-values, *q*-val) are plotted for each genetic locus. Loci with a *q*-val ≤ 0.05 and a log2FC ≤ −1 are colored green. Loci with a *q*-val ≤ 0.05 and a log2FC ≥ 1 are colored red. Selected mutants are annotated (b) Volcano plot representing RNA-seq data from $darG_{Mtb}$-TetON grown in 7H9 medium with low or high ATC. Gene expression log2FC (low ATC/high ATC) and false discovery rate-adjusted *p* values (*q*-values, *q*-val) are plotted for each gene. Color coding is identical that in to (b) (c) $darG_{Mtb}$-TetON was grown in 7H9 medium with or without ATC for 18 days before plating on 7H10 agar + ATC and with or without rifampicin (1 μg/ml). Plotted are the ratios of CFU in + rifampicin to -rifampicin conditions. Data from (a–c) are derived from three independent experiments

In contrast, most other toxins studied in *Mtb* exert a bacteriostatic effect (Singh *et al*., 2010; Tiwari *et al*., 2015; Agarwal *et al*., 2018; Sharrock *et al*., 2018; Tandon *et al*., 2019). This suggests that, among TA systems, $DarG_{Mtb}$ may be an attractive drug target. Indeed, peptides that disrupt the toxin-antitoxin interface have been designed for other *Mtb* TA modules and inhibition of antitoxins could be a promising avenue for tuberculosis treatment in general (Williams and Hergenrother, 2012; Chan *et al*., 2015; Lee *et al*., 2015; Kang *et al*., 2017).

4 | EXPERIMENTAL PROCEDURES

4.1 | Bacterial culture conditions

M. tuberculosis H37Rv and derived strains were cultured in Middlebrook 7H9 medium (BD Difco) containing 0.2% of glycerol, 0.2% of dextrose, 0.5% of BSA (Roche), 0.085% of NaCl, and 0.05% of Tween-80 or tyloxapol, or in Middlebrook 7H10 agar (BD Difco) containing 10% of OADC supplement (BD) and 0.5% of glycerol. Liquid cultures were incubated under static conditions at 37°C with 5% of CO_2. Agar plates were incubated at 37°C. Selection antibiotics were used at the following concentrations: hygromycin (50 μg/ml), kanamycin (25 μg/ml), zeocin (25 μg/ml), and streptomycin (20 μg/ml). ATC was used at 500 ng/ml except where indicated otherwise. For liquid cultures, ATC was replenished 100% every 7 days.

4.2 | Generation of strains

All plasmids were generated using Gateway cloning technology (Life Technologies). The $\Delta darT_{Mtb}$-$darG_{Mtb}$ strain was generated from WT *M. tuberculosis* H37Rv as described in the Results section using recombineering (Gee *et al*., 2012; Murphy *et al*., 2015). For the $DarG_{Mtb}$-pull-down and ChIP-seq experiments, WT or $\Delta darT_{Mtb}$-$darG_{Mtb}$ *Mtb* strains were transformed with an episomal plasmid encoding for $darG_{Mtb}$-*FLAG* under the P750 promoter. WT *Mtb*

transformed with an attL5-integrating vector encoding for FLAG tag alone under the hsp60 promoter served as the negative control for the ChIP-seq and the pull-down experiments. WT *Mtb* transformed with an episomal vector encoding for *dosR-FLAG* under an ATC-inducible promoter (obtained as a gift from Dr. Tige Rustad, Juno Therapeutics) served as the positive control for the ChIP-seq. WT *Mtb* strains transformed with episomal vectors expressing mCherry alone or $DarG_{Mtb}$-mCherry under the P750 promoter were used for microscopy. The $darG_{Mtb}$-TetON strain was generated as described in (Johnson *et al*., 2019). For cross-complementation studies, the $darG_{Mtb}$-TetON strain was transformed with episomal plasmids expressing either $darG_{Mtb}$, codon-adapted $darG_{Taq,}$ or codon-adapted $darG_{Taq}K80A$ under the hsp60 promoter. Expression of $darT_{Taq}$ was achieved by transforming a giles-integrating plasmid encoding codon-adapted $darT_{Taq}$ under an ATC-inducible promoter (P606) into $\Delta darT_{Mtb}$-$darG_{Mtb}$ *Mtb* or $\Delta darT_{Mtb}$-$darG_{Mtb}$ *Mtb* overexpressing $DarG_{Mtb}$-FLAG.

4.3 | Mouse infections

The animal experiments were performed in accordance with National Institutes of Health guidelines for housing and care of laboratory animals and according to institutional regulations after protocol review and approval by the Institutional Animal Care and Use Committee of Weill Cornell Medicine (protocol number 0601441A). Female 7- to 8-week-old C57BL/6 mice (Jackson Laboratory) were infected with ~100 CFU using an inhalation exposure system (Glas-Col). CFU burden of lungs and spleens at each time point was determined by plating dilutions of organ homogenates on 7H10 agar. Four mice were euthanized at each time point for each group.

4.4 | Pull-down of $DarG_{Mtb}$

About 150 ml of mid-log phase *Mtb* culture was washed with PBS containing 0.05% of Tween 80 (PBST), resuspended in lysis buffer + protease inhibitors, lysed with 0.1 mm zirconia beads and incubated with anti-Flag beads. We washed the beads three times with PBS before elution with FLAG peptides. The eluates were analyzed by mass spectrometry. For the DNaseI treatment, anti-Flag beads were incubated with *Mtb* whole-cell lysates overnight, washed five times with PBS, and then, treated with 25 units of DNaseI at 37°C under gentle shaking for 3 hr.

4.5 | Microscopy

Mtb cultures were collected by centrifugation, washed with PBS containing 0.05% of Tween 80 (PBST), fixed with 4% of paraformaldehyde overnight prior to removal from BSL-3 containment and incubated with 5 μM SYTO 13 (Thermo Fisher Scientific) for 5 min for nucleoid labeling. Single cell suspensions were prepared by centrifugation at 800 rpm for 10 min. After spreading on soft agar pads, bacteria were visualized with a DeltaVision image restoration microscope (GE Healthcare), a 100x oil objective and appropriate filter sets. Images were captured with a pco.edge scientific SCOS camera and analyzed with ImageJ (Schneider *et al*., 2012).

4.6 | ChIP-seq of $DarG_{Mtb}$

About 50 ml cultures of *Mtb* overexpressing FLAG-tagged proteins were grown to an OD of 0.8–1.2. For cultures expressing DosR-FLAG, expression was induced by addition of ATC (100 ng/ml) for 4 days before addition of formaldehyde. For cultures expressing $DarT_{Taq,}$ expression was induced by adding ATC (500 ng/ml) for 8 days before addition of formaldehyde. Chromatin immunoprecipitation was performed as in (Minch *et al*., 2015). NGS library preparation was performed using NEBNext Ultra II DNA Library prep kit for Illumina. Samples were sequenced using standard Illumina protocols producing ~40 million 50-bp single-end reads. Reads were aligned to the reference genome using Bowtie 2.3 (Langmead and Salzberg, 2012). BAM alignment files were created, sorted and indexed using SAMtools (Li *et al*., 2009) and viewed in the IGV viewer (Robinson *et al*., 2011). Peak calling was performed using MACS2 (Zhang *et al*., 2008). Computation of differentially bound sites was performed using DiffBind (Stark and Brown, 2011). For ChIP of $DarG_{Mtb}$ under baseline conditions, peaks from $DarG_{Mtb}$-FLAG were compared against the FLAG control. For ChIP of $DarG_{Mtb}$ from cells overexpressing $DarT_{Taq}$, peaks from the +ATC condition were compared against the -ATC condition as control.

4.7 | Western Blots

Rabbit polyclonal antibody for $DarG_{Mtb}$ was generated by GenScript. DlaT antibody (Bryk *et al*., 2002) was a gift from R. Bryk and C. Nathan at Weill Cornell Medicine. All secondary antibodies were purchased from LI-COR biosciences. Protein lysates were prepared by mechanical lysis with 0.1 mm zirconia beads. Unbroken bacterial cells and beads were removed by centrifugation and supernatants were filtered using 0.22 μm spin-X columns prior to removal from BSL-3 containment. Protein lysates were separated using SDS-PAGE and transferred to a nitrocellulose membrane. After washing and incubation with secondary antibodies, proteins were visualized using Odyssey Infrared Imaging System (LI-COR Biosciences).

4.8 | $darG_{Mtb}$-tetON antibiotic susceptibility

$darG_{Mtb}$-tetON cultures were grown to till mid-log phase in 7H9 medium + ATC and washed twice in 7H9 medium -ATC. Washed cultures were diluted to an OD of 0.02 and grown for 6 days in 7H9 medium -ATC to pre-deplete $DarG_{Mtb}$. Pre-depleted cultures were used to inoculate 384-well black plates with clear flat bottoms that contained

a range of ATC/drug concentrations at an OD of 0.01. Drugs were dispensed using an HP D300e Digital Dispenser (Hewlett Packard). The drug dispensing was randomized using the HP Digital Dispenser software (version 3.2.2), and the dimethyl sulfoxide (DMSO) concentration in each well was normalized to 1%–2%. After incubation for 14 days, the optical density (OD_{580}) in each well was read using a SoftMax M2 plate reader. The data were de-randomized using HP Digital Dispenser Data Merge software.

4.9 | *darG*$_{Mtb}$-tetON Tn-seq

darG$_{Mtb}$-tetON cultures were grown to mid-log phase in 7H9 medium + ATC and washed twice in 7H9 medium -ATC. Washed cultures were diluted to an OD of 0.25 and grown for 3 days in 7H9 medium -ATC to pre-deplete DarG$_{Mtb}$. Pre-depleted cultures were transduced with ΦMycoMarT7 phage as previously described (Long *et al*., 2015; Xu *et al*., 2017) and plated on 7H10 agar plates with 0.05% of tyloxapol and ATC at two different concentrations: 15 ng/ml ATC (ATC-low) and 500 ng/ml (ATC-high). Plates were incubated for 21 days before harvesting, extracting genomic DNA and sequencing as described previously (Long *et al*., 2015; Xu *et al*., 2017). Mapping and quantification of transposon insertions was done as described previously (Xu *et al*., 2017). Differentially represented genes were identified using resampling in the TRANSIT analysis platform as described previously (DeJesus *et al*., 2015; Xu *et al*., 2017). We defined genes having a *q*-value of ≤.05 and a log2FC ≥ 1 or log2FC ≤ −1 as significant.

4.10 | *darG*$_{Mtb}$-tetON RNA-seq

darG$_{Mtb}$-tetON cultures were grown to mid-log phase in 7H9 medium + ATC and washed twice in PBS-tyloxapol 0.05%. Washed cultures were diluted to an OD of 0.015 and grown for 7 days in 7H9 medium -ATC (low ATC) or + ATC (high ATC). Total RNA was extracted as described in (Botella *et al*., 2017) and Illumina cDNA libraries were generated using the RNAtag-Seq protocol as described in (Shishkin *et al*., 2015) and (Botella *et al*., 2017) and sequenced on HiSeq 4000 to generate 50 bases paired-end reads. The samples from three independent replicates were processed in two rounds of library preparation and sequencing.

The sequencing reads were cleaned by trimming adapter sequences and low quality bases using cutadapt v1.9.1 (Martin, 2011), and were aligned to a modified *M. tuberculosis* reference genome using BWA v0.7.15 (Li and Durbin, 2009). The original *M. tuberculosis* genome (H37Rv) was retrieved from NCBI (https://www.ncbi.nlm.nih.gov/nuccore/NC_000962.3) and modified to add a 1,303 bp insertion before the stop codon of the gene *darG*$_{Mtb}$. Raw read counts per gene were extracted using HTSeq-count v 0.6.1 (Anders *et al*., 2015). Differential expression analysis was performed using the Agilent GeneSpring software.

4.11 | Measuring mutability of *darG*$_{Mtb}$-tetON

darG$_{Mtb}$-tetON cultures were grown till mid-log phase in 7H9 medium + ATC and washed twice in 7H9 medium −ATC. Washed cultures were diluted to an OD of 0.05 and grown for 18 days in 7H9 medium with or without ATC. Cells were pelleted and plated on 7H10 agar plates with no rifampicin or 1 μg/ml rifampicin. Colonies were counted after ~3–4 weeks of incubation.

ACKNOWLEDGMENTS

We thank T. Yu and J.A. McConnell for assistance with experiments. We thank T. Rustad (Juno Therapeutics) for advice regarding ChIP-seq and for providing the DosR overexpression plasmid. We thank K.G. Papavinasasundaram (University of Massachusetts) and S.A. Shaffer (University of Massachusetts, Mass Spectrometry Facility) for LC-MS/MS analysis. We thank T. Zhang (Genomics Resources Core Facility, Weill Cornell Medicine) for analysis of the RNA-seq data. We thank T. Ioerger for advice regarding transposon sequencing. We thank R. Bryk and C. Nathan (Weill Cornell Medicine) for the DlaT antibody.

AUTHOR CONTRIBUTIONS

All authors contributed to the conception and design of the study. AZ, RW, LB, RS, LZ, JBW, NS, and RSJ contributed to the acquisition and analysis of data. AZ, SE, DS, and RW contributed to the writing of the manuscript. The authors declare no conflict of interest.

DATA AVAILABILITY STATEMENT

Data that support the findings of this study can be found in the Supporting Information of this article. Raw data from the Tn-seq and RNA-seq experiments are deposited under BioProject accession number PRJNA640933 in the NCBI BioProject database (https://www.ncbi.nlm.nih.gov/bioproject/).

ORCID

Anisha Zaveri https://orcid.org/0000-0003-3338-6627

REFERENCES

Agarwal, S., Tiwari, P., Deep, A., Kidwai, S., Gupta, S., Thakur, K. G., *et al*. (2018) System-wide analysis unravels the differential regulation and in vivo essentiality of virulence-associated proteins B and C toxin-antitoxin systems of *Mycobacterium tuberculosis*. *Journal of Infectious Diseases*, *217*, 1809–1820. https://doi.org/10.1093/infdis/jiy109.

Anders, S., Pyl, P. T. and Huber, W. (2015) HTSeq–a Python framework to work with high-throughput sequencing data. *Bioinformatics*, *31*, 166–169. https://doi.org/10.1093/bioinformatics/btu638.

Boshoff, H. I., Reed, M. B., Barry, C. E. 3rd and Mizrahi, V. (2003) DnaE2 polymerase contributes to in vivo survival and the emergence of drug resistance in *Mycobacterium tuberculosis*. *Cell*, *113*, 183–193. https://doi.org/10.1016/S0092-8674(03)00270-8.

Botella, L., Vaubourgeix, J., Livny, J. and Schnappinger, D. (2017) Depleting *Mycobacterium tuberculosis* of the transcription termination factor Rho causes pervasive transcription and rapid death. *Nature Communications*, *8*, 14731. https://doi.org/10.1038/ncomms14731.

Bryk, R., Lima, C. D., Erdjument-Bromage, H., Tempst, P. and Nathan, C. (2002) Metabolic enzymes of mycobacteria linked to antioxidant defense by a thioredoxin-like protein. *Science*, *295*, 1073–1077. https://doi.org/10.1126/science.1067798.

Chan, W. T., Balsa, D. and Espinosa, M. (2015) One cannot rule them all: are bacterial toxins-antitoxins druggable? *FEMS Microbiology Reviews*, *39*, 522–540. https://doi.org/10.1093/femsre/fuv002.

DeJesus, M. A., Ambadipudi, C., Baker, R., Sassetti, C. and Ioerger, T. R. (2015) TRANSIT–A software tool for Himar1 TnSeq analysis. *PLoS Computational Biology*, *11*, e1004401. https://doi.org/10.1371/journal.pcbi.1004401.

DeJesus, M. A., Gerrick, E. R., Xu, W., Park, S. W., Long, J. E., Boutte, C. C., *et al*. (2017) Comprehensive essentiality analysis of the *Mycobacterium tuberculosis* Genome via saturating transposon Mutagenesis. *mBio*, *8*.

Dubnau, E., Chan, J., Raynaud, C., Mohan, V. P., Laneelle, M. A., Yu, K., *et al*. (2000) Oxygenated mycolic acids are necessary for virulence of *Mycobacterium tuberculosis* in mice. *Molecular Microbiology*, *36*, 630–637. https://doi.org/10.1046/j.1365-2958.2000.01882.x.

Eliopoulos, G. M. and Blazquez, J. (2003) Hypermutation as a factor contributing to the acquisition of antimicrobial resistance. *Clinical Infectious Diseases*, *37*, 1201–1209. https://doi.org/10.1086/378810.

Freire, D. M., Gutierrez, C., Garza-Garcia, A., Grabowska, A. D., Sala, A. J., Ariyachaokun, K., *et al*. (2019) An NAD(+) phosphorylase toxin triggers *Mycobacterium tuberculosis* cell death. *Molecular Cell*, *73*(1282–1291), e1288. https://doi.org/10.1016/j.molcel.2019.01.028.

Fudrini Olivencia, B., Muller, A. U., Roschitzki, B., Burger, S., Weber-Ban, E. and Imkamp, F. (2017) *Mycobacterium smegmatis* PafBC is involved in regulation of DNA damage response. *Scientific Reports*, *7*, 13987. https://doi.org/10.1038/s41598-017-14410-z.

Gee, C. L., Papavinasasundaram, K. G., Blair, S. R., Baer, C. E., Falick, A. M., King, D. S., *et al*. (2012) A phosphorylated pseudokinase complex controls cell wall synthesis in mycobacteria. *Science Signalling*, *5*, ra7. https://doi.org/10.1126/scisignal.2002525.

Gerdes, K. and Maisonneuve, E. (2012) Bacterial persistence and toxin-antitoxin loci. *Annual Review of Microbiology*, *66*, 103–123. https://doi.org/10.1146/annurev-micro-092611-150159.

Gerdes, K., Rasmussen, P. B. and Molin, S. (1986) Unique type of plasmid maintenance function: Postsegregational killing of plasmid-free cells. *Proceedings of the National Academy of Sciences*, *83*, 3116–3120. https://doi.org/10.1073/pnas.83.10.3116.

Harms, A., Brodersen, D. E., Mitarai, N. and Gerdes, K. (2018) Toxins, targets, and triggers: an overview of toxin-antitoxin biology. *Molecular Cell*, *70*, 768–784. https://doi.org/10.1016/j.molcel.2018.01.003.

Iyer, V. N. and Szybalski, W. (1963) A molecular mechanism of mitomycin action: linking of complementary DNA strands. *Proceedings of the National Academy of Sciences*, *50*, 355–362. https://doi.org/10.1073/pnas.50.2.355.

Jankevicius, G., Ariza, A., Ahel, M. and Ahel, I. (2016) The toxin-antitoxin system DarTG catalyzes reversible ADP-ribosylation of DNA. *Molecular Cell*, *64*, 1109–1116. https://doi.org/10.1016/j.molcel.2016.11.014.

Johnson, E. O., LaVerriere, E., Office, E., Stanley, M., Meyer, E., Kawate, T., *et al*. (2019) Large-scale chemical-genetics yields new M. tuberculosis inhibitor classes. *Nature*, *571*, 72–78. https://doi.org/10.1038/s41586-019-1315-z.

Jolivet-Gougeon, A., Kovacs, B., Le Gall-David, S., Le Bars, H., Bousarghin, L., Bonnaure-Mallet, M., *et al*. (2011) Bacterial hypermutation: Clinical implications. *Journal of Medical Microbiology*, *60*, 563–573. https://doi.org/10.1099/jmm.0.024083-0.

Kanehisa, M. and Goto, S. (2000) KEGG: Kyoto encyclopedia of genes and genomes. *Nucleic Acids Research*, *28*, 27–30. https://doi.org/10.1093/nar/28.1.27.

Kang, S. M., Kim, D. H., Lee, K. Y., Park, S. J., Yoon, H. J., Lee, S. J., *et al*. (2017) Functional details of the *Mycobacterium tuberculosis* VapBC26 toxin-antitoxin system based on a structural study: Insights into unique binding and antibiotic peptides. *Nucleic Acids Research*, *45*, 8564–8580. https://doi.org/10.1093/nar/gkx489.

Kim, J. H., Wei, J. R., Wallach, J. B., Robbins, R. S., Rubin, E. J. and Schnappinger, D. (2011) Protein inactivation in mycobacteria by controlled proteolysis and its application to deplete the beta subunit of RNA polymerase. *Nucleic Acids Research*, *39*, 2210–2220. https://doi.org/10.1093/nar/gkq1149.

Langmead, B. and Salzberg, S. L. (2012) Fast gapped-read alignment with Bowtie 2. *Nature Methods*, *9*, 357–359. https://doi.org/10.1038/nmeth.1923.

Lawaree, E., Jankevicius, G., Cooper, C., Ahel, I., Uphoff, S. and Tang, C. M. (2020) DNA ADP-ribosylation stalls replication and is reversed by RecF-mediated homologous recombination and nucleotide excision repair. *Cell Reports*, *30*(1373–1384), e1374. https://doi.org/10.1016/j.celrep.2020.01.014.

Lee, I. G., Lee, S. J., Chae, S., Lee, K. Y., Kim, J. H. and Lee, B. J. (2015) Structural and functional studies of the *Mycobacterium tuberculosis* VapBC30 toxin-antitoxin system: implications for the design of novel antimicrobial peptides. *Nucleic Acids Research*, *43*, 7624–7637.

Li, H. and Durbin, R. (2009) Fast and accurate short read alignment with Burrows-Wheeler transform. *Bioinformatics*, *25*, 1754–1760. https://doi.org/10.1093/bioinformatics/btp324.

Li, H., Handsaker, B., Wysoker, A., Fennell, T., Ruan, J., Homer, N., *et al*. (2009) The sequence alignment/map format and SAMtools. *Bioinformatics*, *25*(16), 2078–2079. https://doi.org/10.1093/bioinformatics/btp352.

Long, J. E., DeJesus, M., Ward, D., Baker, R. E., Ioerger, T. and Sassetti, C. M. (2015) Identifying essential genes in *Mycobacterium tuberculosis* by global phenotypic profiling. *Methods in Molecular Biology*, *1279*, 79–95.

Martin, M. (2011) Cutadapt removes adapter sequences from high-throughput sequencing reads. *EMBnet Journal*, *2011*(17), 3. https://doi.org/10.14806/ej.17.1.200.

Minch, K. J., Rustad, T. R., Peterson, E. J., Winkler, J., Reiss, D. J., Ma, S., *et al*. (2015) The DNA-binding network of *Mycobacterium tuberculosis*. *Nature Communications*, *6*, 5829. https://doi.org/10.1038/ncomms6829.

Muller, A. U., Imkamp, F. and Weber-Ban, E. (2018) The Mycobacterial LexA/RecA-independent DNA damage response is controlled by PafBC and the Pup-proteasome system. *Cell Reports*, *23*, 3551–3564. https://doi.org/10.1016/j.celrep.2018.05.073.

Murphy, K. C., Papavinasasundaram, K. and Sassetti, C. M. (2015) Mycobacterial recombineering. *Methods in Molecular Biology*, *1285*, 177–199.

Nebbioso, A., Benedetti, R., Conte, M., Carafa, V., De Bellis, F., Shaik, J., *et al*. (2017) Time-resolved analysis of DNA-protein interactions in living cells by UV laser pulses. *Scientific Reports*, *7*, 11725. https://doi.org/10.1038/s41598-017-12010-5.

Ogura, T. and Hiraga, S. (1983) Mini-F plasmid genes that couple host cell division to plasmid proliferation. *Proceedings of the National Academy of Sciences*, *80*, 4784–4788. https://doi.org/10.1073/pnas.80.15.4784.

Pandey, D. P. and Gerdes, K. (2005) Toxin-antitoxin loci are highly abundant in free-living but lost from host-associated prokaryotes. *Nucleic Acids Research*, *33*, 966–976. https://doi.org/10.1093/nar/gki201.

Pashley, C. A. and Parish, T. (2003) Efficient switching of mycobacteriophage L5-based integrating plasmids in Mycobacterium tuberculosis. *FEMS Microbiology Letters*, *229*, 211–215.

Ramage, H. R., Connolly, L. E. and Cox, J. S. (2009) Comprehensive functional analysis of *Mycobacterium tuberculosis* toxin-antitoxin systems: implications for pathogenesis, stress responses, and evolution. *PLoS Genetics*, *5*, e1000767. https://doi.org/10.1371/journal.pgen.1000767.

Robinson, J. T., Thorvaldsdottir, H., Winckler, W., Guttman, M., Lander, E. S., Getz, G. *et al.* (2011) Integrative genomics viewer. *Nature Biotechnology*, *29*, 24–26. https://doi.org/10.1038/nbt.1754.

Sala, A., Bordes, P. and Genevaux, P. (2014) Multiple toxin-antitoxin systems in *Mycobacterium tuberculosis*. *Toxins (Basel)*, *6*, 1002–1020. https://doi.org/10.3390/toxins6031002.

Schneider, C. A., Rasband, W. S. and Eliceiri, K. W. (2012) NIH Image to ImageJ: 25 years of image analysis. *Nature Methods*, *9*, 671–675. https://doi.org/10.1038/nmeth.2089.

Sharrock, A., Ruthe, A., Andrews, E. S. V., Arcus, V. A. and Hicks, J. L. (2018) VapC proteins from *Mycobacterium tuberculosis* share ribonuclease sequence specificity but differ in regulation and toxicity. *PLoS One*, *13*, e0203412. https://doi.org/10.1371/journal.pone.0203412.

Shishkin, A. A., Giannoukos, G., Kucukural, A., Ciulla, D., Busby, M., Surka, C., *et al.* (2015) Simultaneous generation of many RNA-seq libraries in a single reaction. *Nature Methods*, *12*, 323–325. https://doi.org/10.1038/nmeth.3313.

Singh, A. (2017) Guardians of the mycobacterial genome: a review on DNA repair systems in Mycobacterium tuberculosis. *Microbiology*, *163*, 1740–1758. https://doi.org/10.1099/mic.0.000578.

Singh, R., Barry, C. E., 3rd and Boshoff, H. I. (2010) The three RelE homologs of *Mycobacterium tuberculosis* have individual, drug-specific effects on bacterial antibiotic tolerance. *Journal of Bacteriology*, *192*, 1279–1291. https://doi.org/10.1128/JB.01285-09.

Slayden, R. A., Dawson, C. C. and Cummings, J. E. (2018) Toxin–antitoxin systems and regulatory mechanisms in *Mycobacterium tuberculosis*. *Pathogens and Disease*, *76*(4), https://doi.org/10.1093/femspd/fty039.

Stark, R. and Brown, G. (2011) DiffBind: differential binding analysis of ChIP-Seq peak data. *R Package Version*, *100*,3–4.

Szekeres, S., Dauti, M., Wilde, C., Mazel, D. and Rowe-Magnus, D. A. (2007) Chromosomal toxin-antitoxin loci can diminish large-scale genome reductions in the absence of selection. *Molecular Microbiology*, *63*, 1588–1605. https://doi.org/10.1111/j.1365-2958.2007.05613.x.

Taddei, F., Radman, M., Maynard-Smith, J., Toupance, B., Gouyon, P. H. and Godelle, B. (1997) Role of mutator alleles in adaptive evolution. *Nature*, *387*, 700–702. https://doi.org/10.1038/42696.

Tandon, H., Sharma, A., Sandhya, S., Srinivasan, N. and Singh, R. (2019) *Mycobacterium tuberculosis* Rv0366c-Rv0367c encodes a non-canonical PezAT-like toxin-antitoxin pair. *Scientific Reports*, *9*, 1163. https://doi.org/10.1038/s41598-018-37473-y.

Tiwari, P., Arora, G., Singh, M., Kidwai, S., Narayan, O. P. and Singh, R. (2015) MazF ribonucleases promote *Mycobacterium tuberculosis* drug tolerance and virulence in guinea pigs. *Nature Communications*, *6*, 6059. https://doi.org/10.1038/ncomms7059.

Williams, J. J. and Hergenrother, P. J. (2012) Artificial activation of toxin-antitoxin systems as an antibacterial strategy. *Trends in Microbiology*, *20*, 291–298. https://doi.org/10.1016/j.tim.2012.02.005.

Xu, W., DeJesus, M. A., Rucker, N., Engelhart, C. A., Wright, M. G., Healy, C., *et al.* (2017) Chemical genetic interaction profiling reveals determinants of intrinsic antibiotic resistance in *Mycobacterium tuberculosis*. *Antimicrobial Agents and Chemotherapy*, *61*. https://doi.org/10.1128/AAC.01334-17.

Yamaguchi, Y., Park, J. H. and Inouye, M. (2011) Toxin-antitoxin systems in bacteria and archaea. *Annual Review of Genetics*, *45*, 61–79. https://doi.org/10.1146/annurev-genet-110410-132412.

Yuan, Y. and Barry, C. E., 3rd (1996) A common mechanism for the biosynthesis of methoxy and cyclopropyl mycolic acids in *Mycobacterium tuberculosis*. *Proceedings of the National Academy of Sciences*, *93*, 12828–12833. https://doi.org/10.1073/pnas.93.23.12828.

Zhang, Y., Liu, T., Meyer, C. A., Eeckhoute, J., Johnson, D. S., Bernstein, B. E., *et al.* (2008) Model-based analysis of ChIP-Seq (MACS). *Genome Biology*, *9*, R137. https://doi.org/10.1186/gb-2008-9-9-r137.

SUPPORTING INFORMATION

Additional supporting information may be found online in the Supporting Information section.

How to cite this article: Zaveri A, Wang R, Botella L, et al. Depletion of the DarG antitoxin in *Mycobacterium tuberculosis* triggers the DNA-damage response and leads to cell death. *Mol Microbiol*. 2020;114:641–652. https://doi.org/10.1111/mmi.14571